Panoramic functional gradients across the mouse retina

by

Kseniia Kirillova

January, 2023

A thesis submitted to the
Graduate School
of the
Institute of Science and Technology Austria
in partial fulfillment of the requirements
for the degree of
Master of Science

Committee in charge:

Maximilian Joesch
Gasper Tkacik

The thesis of Kseniia Kirillova, titled *Panoramic functional gradients across the mouse retina*, is approved by:

Supervisor: Maximilian Joesch, ISTA, Klosterneuburg, Austria

Signature: _____

Committee Member: Gasper Tkacik, ISTA, Klosterneuburg, Austria

Signature: _____

Signed page is on file

ISTA Master's Thesis, ISSN: 2791-4585

I hereby declare that this thesis is my own work and that it does not contain other people's work without this being so stated; this thesis does not contain my previous work without this being stated, and the bibliography contains all the literature that I used in writing the dissertation.

I declare that this is a true copy of my thesis, including any final revisions, as approved by my thesis committee, and that this thesis has not been submitted for a higher degree to any other university or institution.

I certify that any republication of materials presented in this thesis has been approved by the relevant publishers and co-authors.

Signature: _____

Kseniia Kirillova
January, 2023

Signed page is on file

Abstract

All visual experiences of the vertebrates begin with light being converted into electrical signals by the eye retina. Retinal ganglion cells (RGCs) are the neurons of the innermost layer of the mammal retina, and they transmit visual information to the rest of the brain.

It has been shown that RGCs vary in their morphology and genetic profiles, moreover they can be unambiguously grouped into subtypes that share the same morphological and/or molecular properties. However, in terms of RGCs function, it remains unclear how many distinct types there are and what response properties their typology relies on. Even given the recent studies that successfully classified RGCs in a patch of the retina [1] and in scotopic conditions [2], the question remains whether the found subtypes persist across the entire retina.

In this work, using a novel imaging method, we show that, when sampled from a large portion of the retina, RGCs can not be clearly divided into functional subtypes. We found that in photopic conditions, which implies more prominent natural scene statistic differences across the visual field, response properties can be exhibited by cells differently depending on their location in the retina, which leads to formation of a gradient of features rather than distinct classes.

This finding suggests that RGCs follow a global organization across the visual field of the animal, adapting each RGC subtype to the requirements imposed by the natural scene statistics.

Acknowledgements

Switching from PhD program to MSc studies and completing it was a very difficult experience for me on many different levels, however I was not alone on this way and I would like to acknowledge everyone who was with me during this time.

First, I would like to wholeheartedly thank my supervisor, Max Joesch. I am very grateful for the chance he gave me to stay at ISTA and complete my degree. I greatly appreciate the patience and dedication with which he had dealt with me throughout the project. I believe I grew as a scientist and as a person under his supervision.

Next, I am thankful to the whole Joesch group for being so friendly and cheerful. Even during my rotations at other labs, I always considered myself a part of the Joesch lab because of how warm they were treating me. Special gratitude goes to Divyansh Gupta, who skillfully taught me everything I know about the project and was a great colleague and a friend throughout the past two years. Thank you for being kind and supportive.

For the fruitful conversations and scientific input, I would like to thank my committee member Gasper Tkacik and Wiktor Mlynarski. Our conversations particularly helped me bring out the excitement for the project.

Apart from my immediate colleagues, I am endlessly grateful to my friends who tagged along with me throughout this at times painful journey. Firstly, I am grateful to the Kondrashov lab, who were my foster lab and my office mates. Without daily support from Sonya, Aygul, Catalin and Petya I would have not managed to stay sane during the past year. Secondly, I thank my PhD cohort friends and Christine, Valentin and Yuri in particular. They had my back even at times when I felt like I did not belong in our cohort anymore. And of course I am very grateful to my closest people Vlad, Paolo, Nikita and Sreyam for listening to my endless rants about me being exhausted and frustrated, supporting and cheering me on, making me laugh and making me feel loved and accepted no matter how I perform in my studies.

Last but not least, I would like to thank myself for pushing and not giving up at the hardest times, for being kind to myself along the way and for letting myself progress at my own pace.

About the Author

Kseniia Kirillova completed a BSc in Biomedical Engineering at the Bauman Moscow State Technical University in Moscow, Russia. During her studies she discovered her interest in neuroscience, and therefore she took a year to do two research internships at EMBL Rome in molecular neuroscience and at EMBL Heidelberg in microfluidics.

This experience led her to later widen her experience in neuroscience at HHMI Janelia Research Campus, USA. Here she discovered the passion for systems and computational neuroscience, which brought her to the ISTA PhD program.

During the first year of PhD studies, her priorities have changed, and therefore she decided to graduate from ISTA with an MSc degree focusing on neuroscience and data science.

Table of Contents

Abstract vii

Acknowledgements viii

About the Author ix

Table of Contents xi

List of Figures xi

List of Abbreviations xiii

1 Introduction 1
- 1.1 Retina anatomy . . . 1
- 1.2 Retina function . . . 3

2 Materials and methods 9
- 2.1 Data acquisition . . . 9
- 2.2 Data preprocessing . . . 9
- 2.3 Clustering into functional types . . . 11
- 2.4 Mapping of RF properties . . . 11

3 Results 13
- 3.1 Functional classification . . . 13
- 3.2 Retinal organizational patterns . . . 21

4 Discussion 25
- 4.1 Functional classification . . . 25
- 4.2 Retinal organizational patterns . . . 27

Bibliography 29

List of Figures

1.1 **Schematic of the anatomy of the mouse retina. a.** Spatial distribution of the two anatomical cone types (green - MS cones; purple - S cones) across the retina (D, dorsal; V, ventral; T, temporal; N, nasal). **b.** Graphical representation of a cross-section of the retina. Legend to the cell types on the right panel. **c.** Mouse brain and the two main downstream targets of the RGCs (SC, superior colliculus; LGN, lateral geniculate nucleus). 2

2.1 **Data acquisition pipeline. a.** Schematic of the recording setup. **b.** Chirp stimulus (on the left) presented by the projector evokes chirp responses in RGCs (in the middle). From raw responses, we calculate the mean response and the quality index (QI) (on the right). **c.** Checker stimulus (on the left) presented by the projector evokes responses in RGCs, from which we calculate spatio-temporal RF (on the right). **d-f.** Spatial, temporal and radial RFs extracted from the recorded spatio-temporal RF. 10

3.1 **Optimal number of clusters estimation. a.** Elbow method for estimating the optimal number of clusters in the spatial Rfs data.**b.** Same for chirp responses. **c.** Same for temporal RFs. **d.** Same for spatial RFs, temporal RFs and chirp responses combined. 14

3.2 **Spatial receptive fields clusters. a.** Projections of spatial RFs in the cluster, from left to right: horizontal, vertical, 45 degrees. **b.** Cluster-mean response properties, left: spatial RF, right: temporal RF, shaded area represents standard deviation. **c.** Distribution of cells from the cluster within the retina, left: density map, right: linear regression weights of density map on elevation (EL) and azimuth (AZ). **d.** Left: chirp responses of cells in the cluster, grouped into 4 clusters for visualization purposes. Right: number of cells in the cluster. For mean spatial RFs and density maps axes: down-up = D-V; left-right = T-N. 16

3.3 **Chirp response clusters. a.** Chirp responses of cells in the cluster. **b.** Cluster-mean response properties, left: spatial RF, right: temporal RF, shaded area represents standard deviation. **c.** Distribution of cells from the cluster within the retina, left: density map, right: linear regression weights of density map on elevation (EL) and azimuth (AZ). **d.** Left: cluster-mean chirp response, shaded area represents standard deviation. Right: number of cells in the cluster, represented with a red bar for ON cells and a blue bar for OFF cells. For mean spatial RFs and density maps axes: down-up = D-V; left-right = T-N. 18

3.4 **Variety of temporal RFs. a.** Temporal RFs of all RGCs in the dataset, grouped into 4 clusters and sorted within each cluster by time of the first peak and time of the second peak combined. **b.** Distributions of timings of the first peak, zero crossing and the second peak. 19

3.5 **Clustering based on dimensionality reduction. a.** UMAP representation of the spatial RFs data. **b.** Same for chirp responses. **c.** Same for temporal RFs. **d.** Same for spatial RFs, temporal RFs and chirp responses combined. 20

3.6 **Comparison of kinetics of ON and OFF cells and changes in kinetics across the retina. a.** OFF:ON cell count ratio. **b.** Distribution of timings of first peak (left panel), zero crossing (middle panel), second peak (right panel) in the temporal RFs of RGCs. **c.** Distributions of relative surround:center strength differ for cells exhibiting high-quality chirp responses and low-quality. **d.** Distributions of QIs of chirp responses differ for ON and OFF cells. **e.** Distributions of relative surround:center strength differ for ON and OFF cells. **f.** Right: map of timing of the first peak in the temporal filter for all RGCs in the dataset. Middle: same for ON cells. Left: same for OFF cells. **g.** Same as f for timing of zero crossing. **h.** Same as f for timing of the second peak. **i.** Same as f for chirp response QI. D, dorsal; V, ventral; T, temporal; N, nasal 24

List of Abbreviations

AbC activated-by-contrast. 25

ACs Amacrine cells. 3

AZ azimuth. 11

BCs Bipolar cells. 2

DS direction selective. 4

DV dorso-ventral. 11

EL elevation. 11

FOV field of view. 6

HCs Horizontal cells. 2

LGN lateral geniculate nucleus. 3

MEA multi-electrode array. 9

NT naso-temporal. 11

PCA principal components analysis. 18

QI Quality Index. 10

RF receptive field. 4

RGCs Retinal ganglion cells. vii, 1

SACs starburst amacrine cells. 4

SbC suppressed-by-contrast. 16

SC superior colliculus. 3

UMAP Uniform Manifold Approximation and Projection. 19

CHAPTER 1

Introduction

Any visual experience begins when light enters the eye and is focused by the cornea and lens onto photoreceptors of the retina. Photoreceptors convert light energy into changes in membrane potential that are transmitted to the interneurons. These interneurons are arranged into multiple circuits that relay the signals to retinal ganglion cells (RGCs). Axons of RGCs form the optic nerve, which sends the information to visual centers of the brain [1].

I am interested in understanding how the retina processes the incoming light and turns it into the neural code. This study uses *Mus musculus* as a model organism to address this question. In the manuscript I will first talk about past knowledge on the anatomy of retina and its function, then the open research questions and lastly my methods to approach these questions, my resulting findings and how they fit into existing theories.

1.1 Retina anatomy

The vertebrate retina is organized into five layers (Fig. 1.1b): (i) photoreceptor layer; (ii) outer plexiform layer; (iii) inner nuclear layer, containing interneurons; (iv) inner plexiform layer; and (v) ganglion cell layer, comprised of retinal ganglion cells that project their axons to diverse visual recipient layers in the brain (Fig. 1.1c). Both of the plexiform layers contain synapses between the cells of the adjacent nuclear layers [3].

Vertebrate retinas utilize two types of photoreceptors - rods and cones. Both hyperpolarize to light, however at different conditions. Rods can sense even single photons and thus are mostly active during night vision, while cones are activated only during the daylight and intermediate lighting conditions [4]. Rods comprise around 97% of all photoreceptive cells in the mouse retina, and they are spread across the whole retina uniformly [5]. Mouse cones can be divided into two types on the basis of the visual pigment, opsin, they express: genuine S cones and MS cones coexpressing both S and M opsins. S opsins are sensitive to short wavelengths in the UV range (360 nm) and M opsins are tuned to medium wavelengths (530 nm). S:M opsin ratio over the whole retina is 3-4:1, making mice able to see mostly in the UV spectrum [4]. Unlike the uniformly spread rods, the cone array features a pronounced dorso-ventral gradient in opsin expression. While genuine S cones make up only 4% of all cones and are homogeneously distributed, MS cones coexpress M and S opsins at different ratios at different parts of the retina. As a consequence, the mouse retina can be divided into three major anatomical regions: (i) the dorsal retina, containing mainly MS cones with very

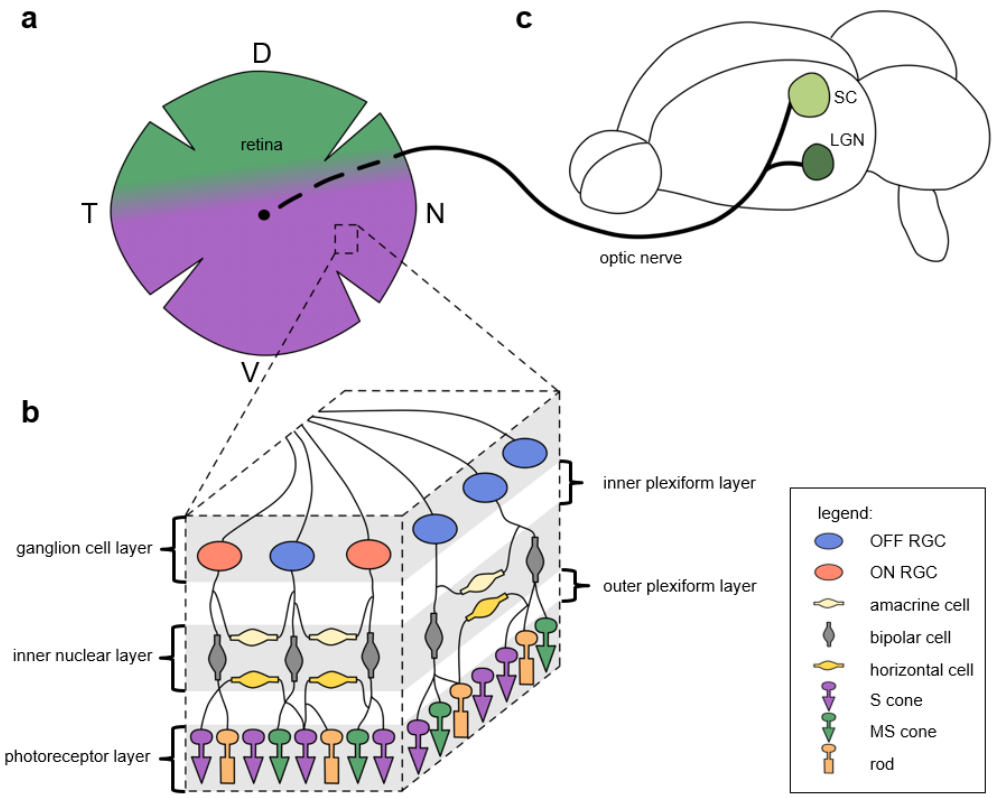

Figure 1.1: **Schematic of the anatomy of the mouse retina. a.** Spatial distribution of the two anatomical cone types (green - MS cones; purple - S cones) across the retina (D, dorsal; V, ventral; T, temporal; N, nasal). **b.** Graphical representation of a cross-section of the retina. Legend to the cell types on the right panel. **c.** Mouse brain and the two main downstream targets of the RGCs (SC, superior colliculus; LGN, lateral geniculate nucleus).

little S opsin coexpression, interspersed with genuine S cones, (ii) a relatively narrow central "opsin transitional zone", in which the S/M opsin coexpression ratio increases, and (iii) the strongly S opsin-dominated ventral retina (Fig. 1.1a) [6].

Both rods and cones synapse onto Bipolar cells (BCs) (Fig. 1.1b). These cells have distinct morphology, as they have two similar protrusions, one receiving signals and one transmitting the output. There exist 14-15 functional BC subtypes, of which one gets inputs from rods and the rest from cones [7]. Since most mammalian retinae are dominated by rod photoreceptors, the rod bipolar cells are the most numerous type of BCs [7]. Instead of making direct connections with retinal ganglion cells, rod BCs feed rod signals into the cone bipolar pathways at the level of cone BC terminals. As a result, the rod signals effectively use the same circuitries that process cone signals [8]. The outputs of different BC types are layered inside the inner plexiform layer and thereby provide synaptic input to distinct sets of RGCs and amacrine cells [9; 7]. The shape, differences in dendritic morphology and inner plexiform layer stratification level of BC's terminals are the main indicators of bipolar cell type identity [7].

Horizontal cells (HCs) mediate lateral interactions in the outer plexiform layer (Fig. 1.1b). They receive light-evoked synaptic input from photoreceptors and hyperpolarize in response to light increments. One can distinguish two types of HCs - the axon-bearing B-type and axonless A-type. However, only the B-type is present in the mouse retina that is of interest to me. Their dendrites receive input from all cones within their dendritic field, while their axon terminal system is postsynaptic to rods [10; 4].

The third type of interneurons in the retina, the Amacrine cells (ACs), receive their excitatory inputs from bipolar cells and make feedback synapses back onto bipolar cell terminals (Fig. 1.1b). They also provide input to RGCs. There exist at least 45 morphologically distinct amacrine cell types (63 types were recently identified molecularly [11]) and all of them operate within the same network of BC's axons and dendrites of RGCs [12]. They collect their excitatory inputs from bipolar cells, onto which they also make feedback synapses. Amacrine cells also make feedforward synapses onto ganglion cell dendrites and lateral inhibitory synapses onto other amacrine cells. Most ACs possess no axon - instead, synaptic outputs come from the same dendrites that receive synaptic inputs, allowing some amacrine cells to perform multiple visual computations in parallel [12].

Retinal ganglion cell bodies form the innermost layer of the retina, while their axons combine into the optic nerve that passes the visual information into the lateral geniculate nucleus (LGN) and the superior colliculus (SC), as well as >40 other brain regions (Fig. 1.1c) [13]. RGCs vary greatly in terms of morphology, gene expression and electrophysiology - in the most recent studies 35-50 cell types were identified based on these characteristics separately or combined [1; 2; 14; 15]. Ideally, RGCs of the same type are expected to share the same physiology, morphology, intra-retinal connectivity, retinal mosaic (the way cells of the same type are distributed within the retina), immunohistochemical profile and genetic markers. Whether these features are necessary and sufficient to define a type and how classification schemes should be organized is a matter of long-standing debate. For example, one could also consider axonal projections to be type-specific, however this would significantly increase the number of cell types [1].

1.2 Retina function

The anatomical complexity of the retina underlies the computational purpose of it. In the mouse retina, there are about 120 million rods and 6 million cones, whilst the output of the retina is transmitted by around 1.2 million retinal ganglion cells [15]. One can assume that within the retina there exist certain information processing rules that allow such downsampling without losing behaviorally relevant information. In the following paragraphs, I will describe the current understanding of the functions of the retina in general and its neurons in particular.

1.2.1 Function of photoreceptors and interneurons

Rods are very sensitive, can reliably transduce the absorption of single photons, and are mostly responsible for vision at low light levels. Cones are less sensitive and are active during daytime vision. Both rods and cones hyperpolarize following an increase in light intensity, and release their transmitter, glutamate [3; 16].

The photoreceptors contact bipolar cells and horizontal cells in the outer plexiform layer and relay their activation downstream. Horizontal cells are thought to mediate feedback inhibition to photoreceptors and feedforward inhibition to bipolar cells [12]. These cells are GABAergic, and they modulate glutamatergic output of cones via parallel feedback mechanisms. Recent electrophysiology studies show that HC feedback can act at the level of a single synaptic contact between an HC dendritic tip and a cone axon terminal. Moreover, pharmacologically removing horizontal cells from the circuitry reduced the sensitivity of the cone signal to low frequencies, suggesting that local horizontal cell feedback shapes the temporal properties of cone output [9]. Additionally, HCs have been implicated in global processing, such as

contrast enhancement and the generation of antagonistic center-surround receptive fields - a fundamental response feature that increases spatial acuity and is present throughout the visual system. It is possible because they mediate lateral signaling that opposes the primary, radial feedforward signal.

Bipolar cells decompose the signal from photoreceptors and HCs into parallel channels, providing the basis for the functional diversity of retinal ganglion cells [9]. Cone bipolar cells can be grouped into ON and OFF cells depending on whether they respond to local light increase or decrease respectively [9]. The topographic stratification of cone BC axons in the inner plexiform layer establishes some of the functional organization of visual processing in the retina: ON BCs are found closer to the ganglion cell layer, and cells with faster responses are segregated towards the border between ON and OFF sublamina. Further differentiation into subtypes is also anatomically enforced by the shape and IPL stratification level of a bipolar cell's terminal system [7]. Functionally, subtypes exhibit different response features such as spectral sensitivity and speed (more transient versus more sustained responses) [9].

Before reaching the ganglion cells, the visual signal goes through another processing step performed by the amacrine cells. These cells are the most heterogeneous retinal class, and are thought to perform specific visual computations that modify the input–output transformations implemented by the excitatory connections between BCs and RGCs [12]. One of the most studied subtypes is called starburst amacrine cells (SACs); it is interesting because its dendrites are strongly activated by visual motion from their somata towards the dendritic tips, but not by motion in the opposite direction, making these cells direction selective (DS). This effect is likely generated by a "dendrite-autonomous" computation on selectively sampled OFF bipolar cell inputs [7; 17]. The downstream ganglion cells also become direction selective after receiving synaptic input from SACs. Another motion sensing (but not DS) subtype of ACs named VG3-AC acts as local edge detectors or object motion sensors, because it can distinguish moving objects from a visual scene that is also moving. These excitatory cells give a selective input to a population of RGCs that inherits its properties and is called W3B-RGC subtype [18]. There also exists a subtype of amacrine cells that is largely involved in scotopic vision via modulating output of rod BCs [12]. Overall, functional roles of amacrine cells vary greatly and are still under investigation.

1.2.2 Function of RGCs and the retina as a whole

The last step of retinal information processing happens in retinal ganglion cells. These cells transmit behaviorally relevant visual information to the rest of the brain. There are many ways to describe the response properties of RGCs. Given the enormous space of stimulus possibilities in the natural world, one can describe them in terms of temporal or spatial properties, direction or orientation selectivity, preference for light increase or decrease, transient or sustained response, etc. However, all these approaches sample only specific aspects of the stimulus space and are in no manner exhaustive. A common way to describe the relationship between the visual stimulus and the spiking activity of RGCs is a receptive field (RF). RF can be defined as a map between spatio-temporal patterns of light and RGC spikes. One can measure either temporal, spatial or spatio-temporal RF. One way of thinking about the temporal changes of an RF is the optimal sequence of light changes that would, on average, evoke an action potential. It is thought that temporal RF acts like a linear filter that a cell applies to the input signal. Additionally, in order to produce a spiking response, cells perform some non-linear transformation. In this work, I use the words filter and RF interchangeably.

On the other hand, spatial properties of the RF are a description of the visual area that can modulate a neuron's response. Spatial RFs usually have a center-surround structure, where the center and the surround have temporal components of opposite sign (ON and OFF). The center component is believed to be driven by direct BC input, while the surround is driven by wide-field ACs and HCs [3; 4]. This, according to the predictive coding theory [19], is an efficient way to remove predictable (redundant) components from the sensory stimulus. Spatio-temporal filters are the fullest description of the cell's kinetics, as they measure what spatially and temporally non-uniform signal causes spiking.

For the purpose of this work, when we refer to temporal RF, we will use only the temporal filter that can be inferred from the mean of center pixels of a spatio-temporal filter. A spatial RF is a snapshot of the same spatio-temporal filter at a chosen moment in time (see Methods section) [20]. Additionally, I refer to cells as ON or OFF based on the sign of their center (which also corresponds to the sign of their first peak in temporal RF).

On top of spatio-temporal RFs, one can measure additional parameters describing activity of RGCs - direction of motion, orientation and color selectivity. Not all cells are selective for these features, but they are important for differentiation of functional cell types. The most full to date functional classification studies were performed by Baden et al. and Goetz et al. [1; 2]. The first study used Ca imaging and four types of visual stimuli: (i) a full-field so-called 'chirp' stimulus to characterize polarity, kinetics and the preference for temporal frequencies and contrasts; (ii) a moving bar to probe for direction and orientation selectivity; (iii) binary dense noise to estimate receptive fields; and (iv) an alternating long- or short-wavelength ('green/blue') full-field stimulus to probe for chromatic preference [1]. The standard chirp stimulus consists of a 1s bright step, increasing amplitude (0 to 127 over 8 s) and increasing frequency (0 to 4 Hz over 8 s), as previously described [6]. The study identified 49 clusters of cells based on all response properties together.

Goetz and colleagues recorded activity of RGCs using cell-attached electrodes [2]. This approach allowed the use of stimuli centered on the receptive field of each cell, as opposed to full-field stimuli used during Ca recordings. The cells were presented with three types of stimuli: (i) round spots of varying sizes to characterize center-surround structure of spatio-temporal RFs; (ii) moving bars to test for direction selectivity; and (iii) drifting gratings for orientation selectivity. Based on these responses, 42 functional clusters were identified.

Clearly defining functional subtypes of RGCs is important for mechanistic understanding of processes in the retina. However, one can also consider the variety of RGCs from the perspective of what it tells us about the function of the retina as a whole. There exist two opposing views on what information the retina conveys to the brain. On the one hand, it was proposed by Lettvin et al. [21] that RGCs serve as feature detectors and mostly react to such properties of the image as local edges and contrast, curvature of edge, motion of edges and dark spots.

The existing functional classification research, including above-mentioned studies by Baden et al. and Goetz et al. look at RGCs only in terms of features that they transmit. This is understandable, because the response properties such as chirp responses, direction and orientation selectivity and responses to bars and spots are showing exactly the feature detection ability of the cells. As a result, current classification of RGCs names classes based on ON-OFFness of the cells and the speed of their response to a flash of light, e.g. 'ON slow/fast', 'OFF alpha sustained/transient', 'ON-OFF local-edge', etc. While this classification reflects certain aspects of RGCs behavior, it could be beneficial to look at retina function from another perspective, that I am describing in the following paragraphs.

The competing (although not necessarily contradicting) hypothesis, known as the efficient coding hypothesis [22; 23], proposes that neural circuits, and the retina in particular, evolved to send a given quantity of information using the least resources. For retina, it mostly means that (i) SNR of the signal given the stochasticity of photons should be balanced against redundancy of cells and synapses; (ii) parallel information processing should be in place to send more information at lower rates, and thus at lower cost in space and energy [24]. These constraints ought to be satisfied by the organization of RGCs. The following paragraphs describe how these constraints are indeed satisfied in the mouse retina.

RGCs, similarly to the bipolar cells, can be roughly divided into ON and OFF types [3]. Firstly, it is known that there are twice as many OFF bipolar cells compared to ON [25]. Therefore, there is a comparable ratio of OFF and ON RGCs. At the same time, OFF RGCs have denser dendritic arbors and their array has more synapses, meaning that an individual OFF cell uses the same resources as an ON cell, but it reads information from a smaller region of the scene. Overall, the OFF cells together use more total resources to represent a scene compared to the ON array [24]. Under the assumption that the retina is optimizing its energy use, this suggests that negative contrasts need to be represented more, which is indeed predicted from the analysis of natural scene statistics because natural scenes contain more of dark regions [26].

All the visual information could potentially be transmitted by just generic ON and OFF RGCs without any further differentiation into subtypes. However, the energetic cost of this kind of signaling would be too high, because it would require more spikes and given that synaptic transmission is the most metabolically expensive type of neural signaling. It has been shown that metabolic cost is minimized when signals are distributed over multiple weakly active cells [24]. Therefore, there exist several cell types tuned to particular aspects of the scene and responding with different firing patterns.

1.2.3 Research questions

Classification of RGCs into cell types has been reliably done based on morphology and genetic profiles [2]. The functional classification has been attempted as well [2; 1]. However, all the existing studies sample a relatively small field of view (FOV) of the retina and given that photoreceptor and some interneuron types are not distributed uniformly across the retina, one could hypothesize that downstream processing could be happening differently in different parts of the retina as well, including at the level of RGCs. Sampling from a bigger FOV has not been possible until now because multiphoton imaging approaches can measure cells only at a moderate throughput (ca. 150 RGCs at a time) and multi-electrode array recordings are limited by the recording area of the electrode array [27]. I would like to study functional clustering of RGCs that are sampled from a large FOV and ask if the functional clusters detected in a larger population of RGCs differ from those discovered before. Moreover, it is interesting to me how cells of different subtypes are arranged within the retina and how that arrangement would support the functions of the retina.

Apart from sampling a bigger FOV, I would also like to perform functional classification based on response properties that have not been used before. Previous works utilizing Ca imaging have described clustering of RGCs based on their combined responses to chirp stimuli, direction selectivity, color selectivity, temporal RF and size of the center of spatial RF [1] or based on temporal receptive fields only [27]. However, it has not been possible to reconstruct a clear surround structure, while it is as important as the center for describing RGC functional

properties. In this work, I would like to define functional cell types based on high-resolution spatial RFs obtained using novel methodology as described in [27], temporal RFs and their response to a standardized chirp stimulus.

CHAPTER 2

Materials and methods

2.1 Data acquisition

Our research questions required a high-resolution dataset of RGCs activity in both spatial and temporal domains. Existing recording methods such as multiphoton imaging, patch clamp and multi-electrode array (MEA) recording either lack needed throughput or allow limited recording area. Therefore, the dataset was obtained by Divyansh Gupta using the custom-built high-throughput epi-fluorescent imaging setup as described in [27].

In brief, we used a transgenic mouse line Vglut2-ires-cre that expresses red-shifted Calcium indicator RCamp1.07 so as to assess the activity of RGCs specifically [28]. The dark-adapted retina was isolated and flat-mounted, positioned into the experimental apparatus while constantly oxygenated with AMES medium. The indicator's excitation wavelength overlaps with rod and M opsin absorption spectra, however it does not overlap with the S opsin absorption spectrum. Therefore, we could stimulate the retina with a UV-LED projector (405 nm) while simultaneously exciting the indicator with 580 nm light and collecting the responses at 600 nm (Fig. 2.1a).

The recording setup has the advantage of recording a large field of view of 1.7 mm^2 at 10 fps and 1.1 μm/pixel resolution, and it allows to consequently obtain several FOVs from the same retina without quality loss. At the same time, it is important to note that the recording can happen only at photopic conditions and only in the monochrome (UV) light. Additionally, as with any Ca-imaging, one can not record single action potentials. Lastly, the range of stimuli is limited to full-field as opposed to centering stimuli of smaller size at each cell's RF.

Each retina was tiled by recording 3-7 FOVs. The final dataset consists of 26558 RGCs from 9 retinas. The recording included 15 minutes of a shifting spatio-temporal noise stimulus with checker size of 100 x 100 μm^2 and 6 Hz update (Fig. 2.1c), followed by a 'chirp' stimulus repeated 5 times (Fig. 2.1b) and a moving bar stimulus repeated 5 times. ROIs were detected automatically from raw calcium movies using Suite2p [29]. Fluorescence traces were then detrended.

2.2 Data preprocessing

Stimulus generation and data preprocessing was performed using Matlab and Psychtoolbox [30].

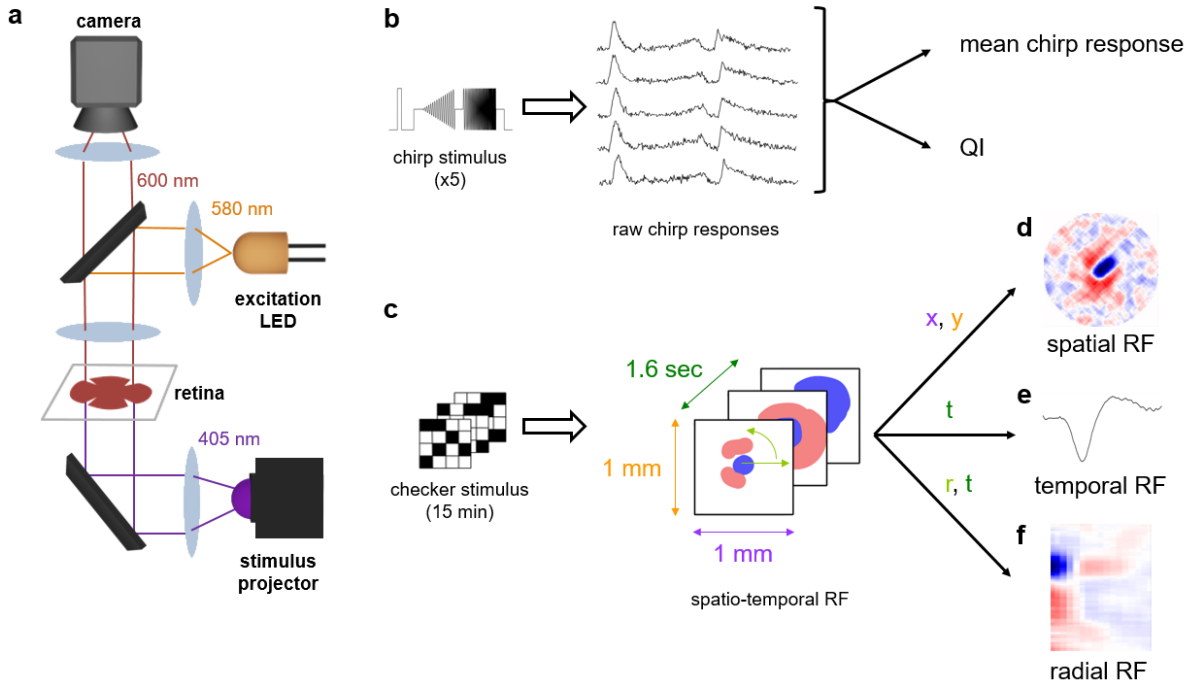

Figure 2.1: **Data acquisition pipeline. a.** Schematic of the recording setup. **b.** Chirp stimulus (on the left) presented by the projector evokes chirp responses in RGCs (in the middle). From raw responses, we calculate the mean response and the quality index (QI) (on the right). **c.** Checker stimulus (on the left) presented by the projector evokes responses in RGCs, from which we calculate spatio-temporal RF (on the right). **d-f.** Spatial, temporal and radial RFs extracted from the recorded spatio-temporal RF.

The mean response across chirp repetitions 2-4 was taken as the response to the chirp because trial 1 usually differs significantly as the retina is not adapted yet after the checkerboard stimulus. The mean response is then zero centered based on the first five data points. We introduced a measure of responsiveness of the cell called Quality Index (QI). It is a quantification of how strongly a given cell was responding to the stimulus in comparison with the noisiness of the response. It also takes into account how well a cell reproduced its response across the 5 trials. Quality Index was computed as in 8, and only responses with QI > 0.45 were used for clustering of chirp responses (Fig. 2.1b).

Novel shifting checkerboard stimuli responses were used to compute spatio-temporal receptive fields as described in [27] (Fig. 2.1c). The resulting temporal component has a sampling frequency of 40 Hz and duration of 1.6 s (Fig. 2.1e). The spatial component was centered for each cell to the pixel of maximum variance, and then cropped within a square window of 1 mm^2 (Fig. 2.1d).

To capture the change of the spatial RF over time, I introduced the radial RF. It was computed as follows: spatio-temporal RF of shape 101x101x64 was cropped to 70x70x64 centered at the original center point, then downsampled by leaving out every second value in both spatial dimensions, resulting in 35x35x64 values. This spatio-temporal RF was then radially scanned, meaning that for each time point 17 concentric circles of radii 1 to 17 pixels were taken around the center point (corresponding to the center point of the center of spatial RF) and for each circle the mean value of all data points on this circle was computed. The resulting radial RF is an array of shape 17x64 (Fig. 2.1f).

2.3 Clustering into functional types

All data analysis was done using Python and standard libraries (numpy, pandas, matplotlib) unless stated otherwise.

Dimensionality reduction was performed using UMAP technique implemented with cuML library for Python (RAPIDS framework) [31; 32]. It allows computing UMAP entirely on GPU, which significantly reduces the computational time.

Clustering of raw data was performed using k-means algorithm implemented with scikit-learn library for Python [33]. The elbow method to estimate the optimal number of clusters was performed with 5-fold cross validation; the sum of distances to the cluster center value for each number of clusters was calculated as the mean of these values in each cross validation run [34]. Cross validation was also implemented with scikit-learn library for Python [33].

Temporal RFs were not clustered, but instead were sorted using Pandas library for Python.

2.4 Mapping of RF properties

For 2-d bins, the retinal space between the outermost recorded cells in both naso-temporal (NT) and dorso-ventral (DV) axes was divided into a square grid and all neurons within each grid were collected.

For density maps of clusters, the density of neurons belonging to each cluster was calculated as a 2-d histogram with a square grid of 30x30 bins, yielding bin size to be approximately 110x110 μm. The resulting density maps were then divided by a density map of all the neurons in the dataset. These normalized for sampling bias density maps were visualized without smoothing in Fig. 4c and 5c. Linear regression weights of each cluster density on elevation (EL) and azimuth (AZ) were computed with scikit-learn library for Python [33]

For OFF:ON ratio mapping, the numbers of neurons of both types were calculated within a square grid of 20x20 bins, yielding bin size to be approximately 165x165 μm. Only 2-d bins with at least 7 ON and 7 OFF neurons were analyzed to minimize sampling bias. This map was visualized without smoothing in Fig. 3.6a.

For temporal RF parameter mapping and chirp QI mapping, the parameter values of neurons were averaged within a square grid of 50x50 bins, yielding bin size to be approximately 65x65 μm. The resulting parameter maps were visualized without smoothing in Fig. 3.6f-i.

CHAPTER 3

Results

3.1 Functional classification

3.1.1 Clustering with k-means

Since spatial RF is a high-dimensional data with 10 201 dimensions (101x101 pixels), for the sake of ease of visual inspection and for the analysis we chose to reduce the dimensionality in a controlled manner. For that, we represented each image as a 1D vector consisting of projections of the spatial RF onto 3 axes - horizontal, vertical and 45 degree. Projection in our case is a sum onto the chosen axis. This representation allows plotting thousands of spatial RF in one plot, while preserving most of the information about the shape of the center and the surround.

K-means clustering is an unsupervised learning algorithm that groups data based on each point Euclidean distance to a central point called centroid. The centroids are defined by the means of all points that are in the same cluster. The algorithm first chooses random points as centroids and then iterates adjusting them until full convergence.

Number of clusters is a hyperparameter that needs to be chosen manually. However, there are metrics to evaluate the quality of clustering for each number of clusters. A rule of thumb for this method says that the optimal number of clusters k $= \sqrt{n/2}$, where n is the number of data points [34]. In our case, this rule is not applicable because it does not make a biological sense to have $\sqrt{26558} = 162$ clusters, given that the previous findings suggest that there are at most 50 functional subtypes.

Another approach is called the "elbow method" [34]. The idea is to calculate the variation explained by the model (the ratio of between cluster variance over total variance) for increasing number of clusters and choose the maximum number after which the variation value plateaus. We performed estimation of the optimal number of clusters with the elbow method with 5-fold cross-validation (Fig. 3.1a-d). The results suggest that there are optimal numbers of clusters for spatial RFs, chirp responses, and temporal RFs, but they range between 10 and 20, which is not in accordance with the previous findings. However, we chose to further evaluate different numbers of clusters by eye.

I chose to cluster first peak spatial RF projections into 20 clusters, as it was in accordance with the elbow method output and also seemed to produce reasonably differentiable clusters (Fig.

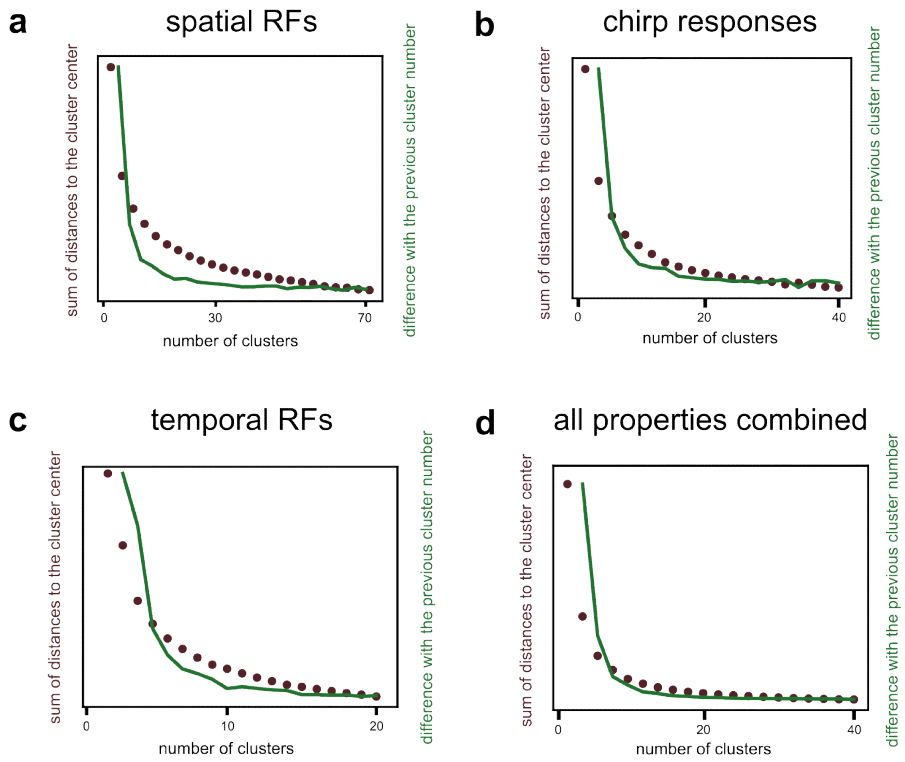

Figure 3.1: **Optimal number of clusters estimation. a.** Elbow method for estimating the optimal number of clusters in the spatial Rfs data.**b.** Same for chirp responses. **c.** Same for temporal RFs. **d.** Same for spatial RFs, temporal RFs and chirp responses combined.

3.2a). However, it is important to note that splitting into any number of clusters between 10 and 60 produced differentiable clusters when inspected by eye.

Previous classification studies such as [1] cluster RGCs based on several response properties combined. However, I wanted to first see how the properties are related to each other and what we can learn about their distribution across the retina. Therefore, after clustering spatial RF projections, for each cluster I then calculated a mean spatial RF (Fig. 3.2b, left column), mean temporal RF (Fig. 3.2b, right column), visualized all the chirp responses (Fig. 3.2d) and also depicted a density map of cluster cells location in the retina subtracting from it the density map of all cells in the dataset (Fig. 3.2c). This approach allows one to clearly see the areas where the given cluster is more densely located than it would be by chance. In order to quantify biasedness in cluster location, I computed linear regression weights of cluster density on elevation (EL) and azimuth (AZ) (Fig. 3.2c, right column).

Since RFs are believed to act as filters that RGCs apply on the input signal, it was interesting to assess whether chirp responses of cells with same spatial RFs are also the same. Therefore, when visualizing chirp responses of cells from each cluster, I also clustered the chirp responses within each cluster into 4 clusters using k-means to highlight the variability of the responses (Fig. 3.2d, right column).

The result shows that the algorithm does indeed pick up different features of spatial RFs, including spatial RF asymmetry (e.g. clusters 4, 12, 17 (Fig. 3.2b, left column)), and separates the clusters reasonably well, such that they look different. Kinetics of the cells looks very uniform across clusters and only ON and OFF clusters are different from each other (Fig. 3.2b, right column). Some clusters show clear bias in location (e.g. clusters 2, 4, 6-9, 12, 17 (Fig.

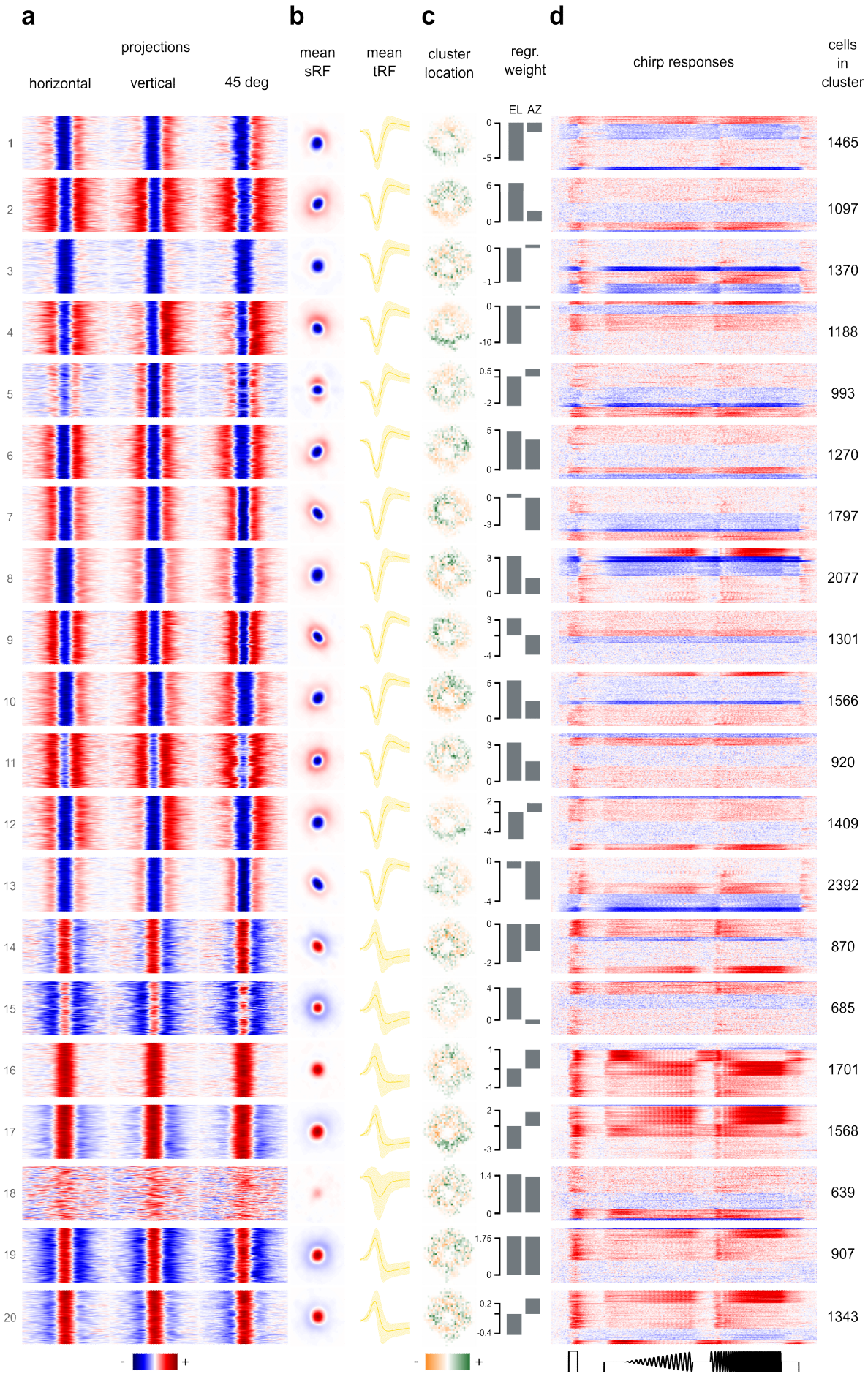
a
b
c
d
projections
horizontal
vertical
45 deg
mean sRF
mean tRF
cluster location
regr. weight
EL AZ
chirp responses
cells in cluster
1 1465
2 1097
3 1370
4 1188
5 993
6 1270
7 1797
8 2077
9 1301
10 1566
11 920
12 1409
13 2392
14 870
15 685
16 1701
17 1568
18 639
19 907
20 1343
- +
- +

3.2c, left column)), whereas the majority is spanned across the whole retina (e.g. clusters 3, 14, 18, 19 (Fig. 3.2c, left column)).

Interestingly, the chirp responses vary greatly within clusters: many clusters include non-responsive, activated-by-contrast and suppressed-by-contrast cells at the same time (Fig. 3.2d). This suggests that clustering by chirp responses could show other potentially interesting patterns. Moreover, it could be more accurate to cluster cells based on both spatial RFs and chirp responses combined.

We then performed the same clustering procedure with the chirp responses that passed our quality criterion (Fig. 3.3). For each cluster we again computed mean spatial RF, temporal RF and cell locations (Fig. 3.3b-c). Since it was obvious that many of the clusters contain both ON and OFF cells, we additionally computed the proportions of these different types (Fig. 3.3d, right column). The rightmost panel shows the mean chirp response of the cluster (Fig. 3.3d, left column).

I chose 20 clusters for visualization ease and following the elbow method results (Fig. 3.1b), even though the clusters do not seem completely uniform (Fig. 3.3a, see clusters 5, 6, 16 for example). This emphasizes how tricky it is to find an optimal number of clusters when using k-means algorithm, because, when inspecting by eye, regardless of how many clusters one splits the data into, they seem sufficiently distinct from each other and at the same time have noticeable within cluster variability. Perhaps, in case of chirp responses one could achieve clustering with less variability within clusters, but this was not necessary because with this clustering I wanted to study only what other response properties do cells with similar chirp responses have, and 20 clusters was enough for it.

The easily noticeable result of clustering is that each chirp cluster contains both ON and OFF cells in different proportions (Fig. 3.3d, right column) leading to the temporal RFs within the majority of clusters varying greatly. This fact points towards the idea that cells also apply various nonlinear filters to the input signal, rather than using only temporal RFs (or spatio-temporal RFs) as linear filters to produce responses.

Strikingly, this analysis revealed that suppressed-by-contrast (SbC) cells, that reduce rather than increase firing rates in response to light increments and decrements, (clusters 16-20) are predominantly OFF cells, whereas activated-by-contrast (clusters 1-15) are mostly ON. Another interesting finding is that, unlike spatial RF clusters, chirp clusters mostly exhibit salt-and-pepper kind of distribution within the retina (Fig. 3.3c, right column).

Overall, the conclusion from this analysis would be similar to spatial RF clustering - one response property is not enough for functional clustering. A combination of several properties is required. However, before combining different response properties, I was curious to also explore the temporal profiles and how variable the kinetics of RGCs can be.

Figure 3.2 *(preceding page)*: **Spatial receptive fields clusters. a.** Projections of spatial RFs in the cluster, from left to right: horizontal, vertical, 45 degrees. **b.** Cluster-mean response properties, left: spatial RF, right: temporal RF, shaded area represents standard deviation. **c.** Distribution of cells from the cluster within the retina, left: density map, right: linear regression weights of density map on elevation (EL) and azimuth (AZ). **d.** Left: chirp responses of cells in the cluster, grouped into 4 clusters for visualization purposes. Right: number of cells in the cluster. For mean spatial RFs and density maps axes: down-up = D-V; left-right = T-N.

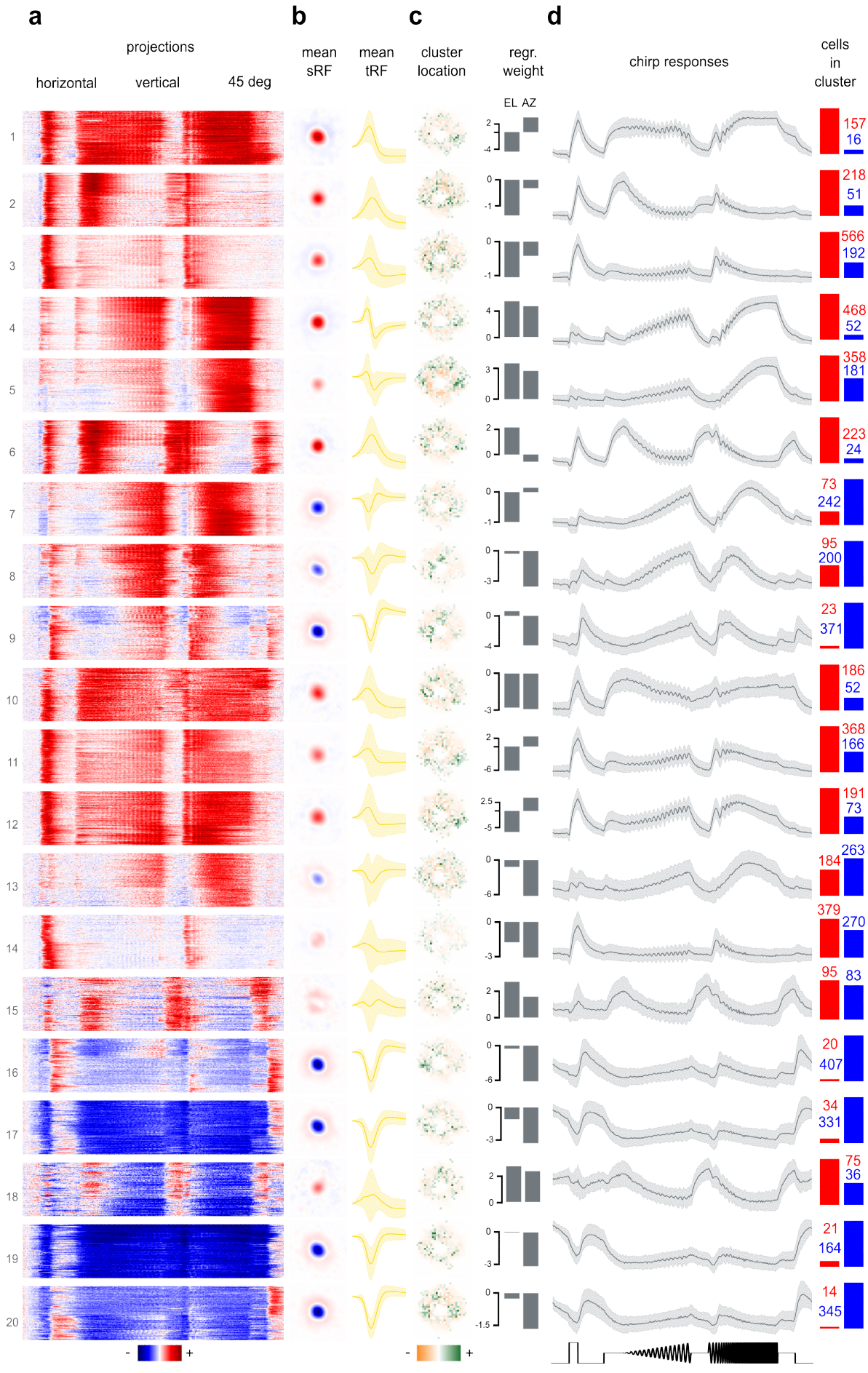
a
b
c
d
projections
horizontal
vertical
45 deg
mean sRF
mean tRF
cluster location
regr. weight
EL AZ
chirp responses
cells in cluster
1 157 16
2 218 51
3 566 192
4 468 52
5 358 181
6 223 24
7 73 242
8 95 200
9 23 371
10 186 52
11 368 166
12 191 73
13 184 263
14 379 270
15 95 83
16 20 407
17 34 331
18 75 36
19 21 164
20 14 345
- +
- +

To study the temporal RFs I chose a slightly different approach, and instead of searching for clear clusters I defined characteristic parameters of temporal filters and sorted the filters according to those (Fig. 3.4a). Firstly, I, however, used k-means to divide temporal RFs into 4 major clusters. We then measured three main temporal RF parameters - time of the first peak (usually it is also the largest peak), time when the filter is crossing zero and time of the second peak. Within each major cluster, the filters were sorted by time of the first peak and time of the second peak combined.

While first peak timing does not vary much (Fig. 3.4b, orange distribution), cells that have the same first peak time vary in their zero crossing and second peak time dramatically and there are all kinds of combinations of these three parameters among all cells. This suggests that temporal RFs also form continuous gradients of properties rather than distinct classes.

Even though spatial RFs, chirp responses and temporal filters did not exhibit clear clusters, I tried to combine these response properties and perform clustering with this data. The elbow method estimated the optimal number of clusters to be around 10 (Fig. 3.1d), which is in no way close to the number of RGC subtypes found in previous studies [1; 2]. Consequently, visualizing clusters did not reveal clearly differentiable clusters (data not shown).

I then hypothesized that radial RF could be the response property that fully represents the ability of RGCs to respond to complex spatial stimuli. Similarly to the study of Goetz et al. [2], which used spots of changing sizes to probe RGCs, radial RFs reflect kinetics of cells not only in the center of their receptive field, but also of their surround. However, the results of k-mean clustering were very similar to those of the other response properties and did not reveal any clusterization (data not shown). This further strengthened my hypothesis that there are no functional subtypes among RGCs.

3.1.2 Clustering based on dimensionality reduction methods

Since k-means clustering did not reveal distinct functional classes of RGC, it was interesting to explore the structure of our data with dimensionality reduction techniques. I hypothesized that k-means could have been not an appropriate clustering method and dimensionality reduction could potentially show clusters as it did in [2]. In this section, I am explaining the choice of an appropriate dimensionality reduction technique and presenting the output of the chosen technique.

There exist two classes of dimensionality reduction techniques - those that focus on preserving the pairwise distance structure amongst all the data samples and those that preserve local over global distance. The most basic technique from the former group is principal components analysis (PCA) which finds projections of the data onto the axes representing most of the variability. PCA is widely used for separating signal from noise, however, it is a suboptimal for dataset with non-linear structure because it is a linear method. Our data potentially has a

Figure 3.3 *(preceding page)*: **Chirp response clusters. a.** Chirp responses of cells in the cluster. **b.** Cluster-mean response properties, left: spatial RF, right: temporal RF, shaded area represents standard deviation. **c.** Distribution of cells from the cluster within the retina, left: density map, right: linear regression weights of density map on elevation (EL) and azimuth (AZ). **d.** Left: cluster-mean chirp response, shaded area represents standard deviation. Right: number of cells in the cluster, represented with a red bar for ON cells and a blue bar for OFF cells. For mean spatial RFs and density maps axes: down-up = D-V; left-right = T-N.

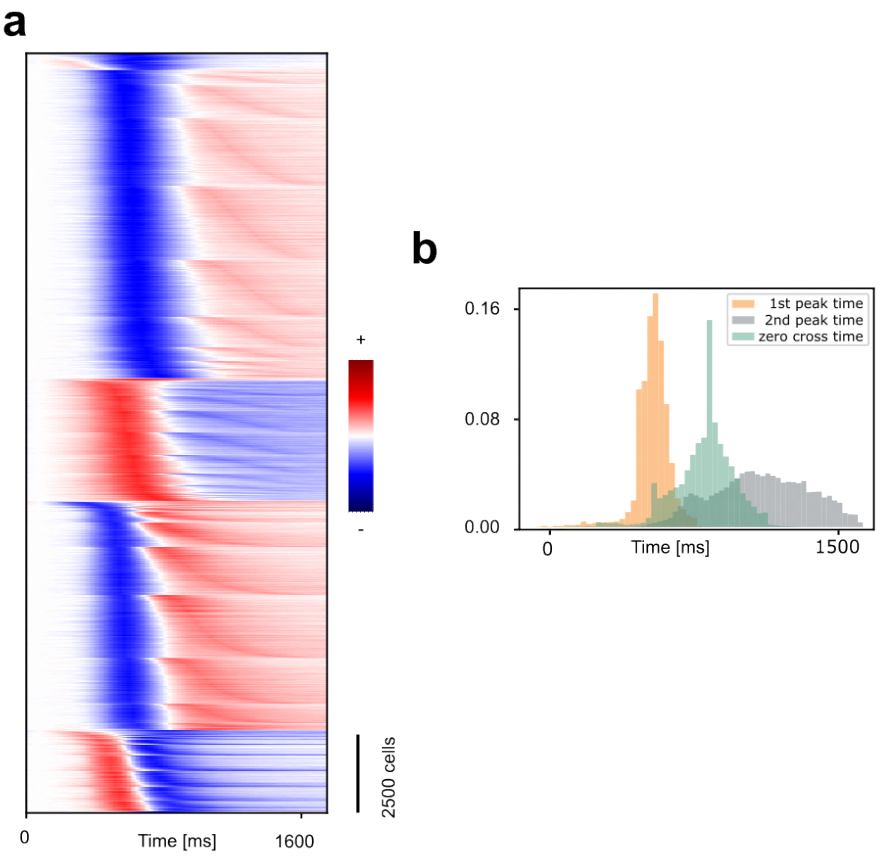

Figure 3.4: **Variety of temporal RFs. a.** Temporal RFs of all RGCs in the dataset, grouped into 4 clusters and sorted within each cluster by time of the first peak and time of the second peak combined. **b.** Distributions of timings of the first peak, zero crossing and the second peak.

non-linear structure, because each spatial RF, as well as temporal RFs and chirp responses, could be a combination of different features that are pronounced at different levels among cell types. As opposed to cells clearly falling into a particular cluster with a defined mean value and variance of some feature, it could be that there is a continuous spectrum of features that span across the features dimensions non-uniformly, similarly to single-cell RNA-seq data [35]. Linear methods would not be able to pick up this sort of structure.

Uniform Manifold Approximation and Projection (UMAP) is a novel manifold learning technique for dimensionality reduction [31]. It has no computational restrictions on embedding dimension, making it a suitable dimension reduction technique for our dataset. It could allow if not immediate functional clustering of cells, then at least visualization of the underlying structure of our data.

After trying UMAP on spatial RFs (Fig. 3.5a), temporal RFs (Fig. 3.5c), chirp responses (Fig. 3.5b) and all these response properties combined (Fig. 3.5d), we can conclude that there are only a few clearly determined clusters. The clusters the algorithm managed to pick up were for spatial RFs, temporal RFs and for all properties combined. Spatial RFs and all properties combined split into ON and OFF groups - those are represented by two clouds in

Fig. 3.5a,d, where the bigger cloud contains OFF cells and the smaller contains ON cells (data not shown). This looks as expected, because it is known that there are about 3 times more OFF cells compared to ON. Temporal filters formed 4 clouds in the UMAP representation. When inspected by plotting means of each of the clouds (data not shown), it turned out that these clusters are ON and OFF cells with strong first peak and weak second peak (monophasic filters), and ON and OFF cells with two strong peaks (biphasic filters), with monophasic OFF being the biggest cloud of all four.

The output of dimensionality reduction algorithms otherwise was not interpretable, because it is unclear what features of the data it picked up as representative of this data's structure. I concluded that it would be interesting to overlay the results from k-means clustering.

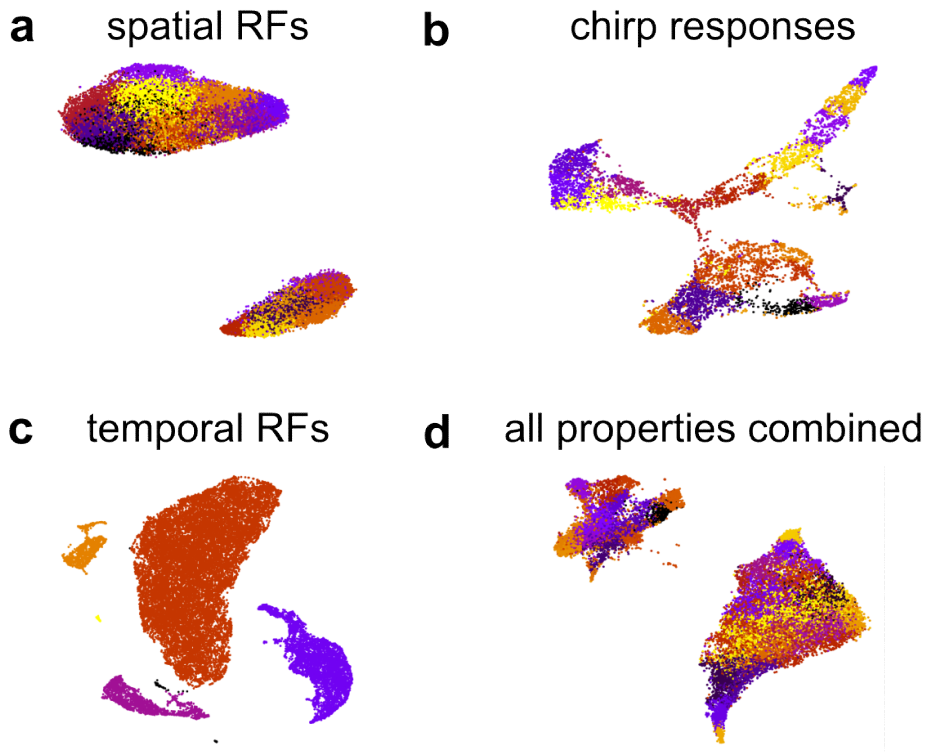

Figure 3.5: **Clustering based on dimensionality reduction. a.** UMAP representation of the spatial RFs data. **b.** Same for chirp responses. **c.** Same for temporal RFs. **d.** Same for spatial RFs, temporal RFs and chirp responses combined.

Since the k-means algorithm picked up somewhat differentiable clusters in the raw spatial RF data and the UMAP representation of the same data did not show any clusters at all, excluding the most obvious ON and OFF cell types, I wanted to see how the clusters found in spatial RF projections by k-means would align with the spatial RFs reduced to 2 dimensions using UMAP. For that, I color coded the data points in the UMAP plot according to cluster numbers in Fig. 3.2. The clusters significantly overlap, but cells from each cluster are located in close proximity to each other (Fig. 3.5a). It suggests that the clusters that k-means picks up might not be clearly separated, and rather represent different parts of one big gradient of features.

Similarly to the clustering of spatial RFs, I aligned chirp clusters identified by k-means with UMAP representation of all the chirps (Fig. 3.5b). The clusters do not overlap much, however

in the UMAP feature space they blend with each other into one big cloud, again suggesting that k-means clusters are enforced on the data.

For temporal RFs, UMAP representation showed 4 clear clusters (Fig. 3.5c), therefore I applied k-means clustering with 4 clusters to raw data and color coded these 4 clusters in the UMAP plot. The clusters found by k-means mostly coincided with the visible UMAP clusters.

Similarly to all the previous analysis, I performed k-means clustering of all response properties combined into 40 clusters and color coded the clusters on the UMAP plot. The result confirmed that all clusters overlap and mix together, although data points from the same clusters are located in close proximity to each other (Fig. 3.5d).

In summary, in our dataset, we cannot find any clear functional clustering. Therefore, our data indicates that RGCs types form functional gradients of different response properties across the entire retina. According to the efficient coding of natural images and the modeling predictions [27], we expect these properties to be unevenly distributed across the retina, which is why in the next part of this work I present our findings on how different spatio-temporal properties of RGCs are represented in different parts of the retina.

3.2 Retinal organizational patterns

It has been shown previously that spatial RFs are organized within the retina in accordance with the efficient coding hypothesis[27]. The main findings include that relative surround strength increases from dorsal to ventral retina, the center size is larger below the horizon level (dorsal retina) and the surrounds have stronger vertical asymmetry below the horizon level such that the top of the surround is stronger than the bottom. The results also indicate that the majority of the cells follow a panoramic organization of spatial RFs. However, it is unknown whether and how other response properties (e.g., temporal RFs and chirp responses) systematically change across the visual field. The following chapter is shedding light onto these questions.

3.2.1 Functional classes of RGCs differ in their distribution bias

Although in the previous chapter we concluded that spatial RFs alone are not sufficient to assign a RGC to a functional cluster, the findings about distribution of different clusters of RGCs with similar spatial RFs are relevant for studying retinal organizational patterns. We identified 4 clusters of spatial RFs with pronounced vertical asymmetry (clusters 4, 10, 12, 17 (Fig. 4b, left column)) that also show a skewed distribution along the ventral-dorsal axis (Fig. 4c, left column). Their distribution is in accordance with previous findings [27].

Another interesting group of clusters that were not described previously, are clusters 6, 7, 9, 13 and 14, that have their centers and surround elongated along diagonal axes (Fig. 3.2b, left column). Their location in the retina seems to have an oval shape elongated along the same axis as the cluster's spatial RF (Fig. 3.2c, left column). These clusters together have 7630 cells (28.7% of the dataset) and therefore must also produce an overall effect on the activity of the retina, which could be studied in more detail.

In contrast to spatial RFs, clusters of chirp responses mostly do not show clear and interpretable distribution patterns. Little is also known about temporal profiles organization patterns.

3.2.2 Distribution of temporal properties in the retina

The two most distinguishable types of RGCs are ON and OFF cells. I hypothesized that their kinetics could be different, and they should be studied separately. It is known that there are roughly twice as many OFF RGCs compared to ON cells in the retina, and I decided to firstly test whether this ratio is constant across the whole retina.

The OFF:ON ratio varies from 1:1 to as much as 4:1 in different locations, while the region with the highest ratio is ventro-temporal (Fig. 3.6a).

I then investigated the kinetics of temporal filters of ON and OFF cells by comparing the distributions of timings of first peak, zero crossing and second peak (Fig. 3.6b). While the 1st peak time has close means and low variance for both distributions (Fig. 3.6b, left panel), zero crossing time happens on average later for OFF cells and ON cells seemingly have 2 populations of cells with faster and slower kinetics (Fig. 3.6b, central panel). Timing of 2nd peak is also on average later for OFF cells and ON cells have a significant population of fast cells and a uniform tail of slower cells (Fig. 3.6b, right panel).

The spatial distribution of cells with different kinetics was assessed for all cells together (Fig. 3.6f-h, left panel) and the ON and OFF cells separately (Fig. 3.6f-h, middle and right panels respectively). For all three characteristic time points the overall distribution is similar with a gradient from slower to faster cells from dorso-temporal to ventro-nasal parts of the retina (Fig. 3.6f-h, left panel). For zero crossing and second peak times the overall gradient repeats the gradient seen among OFF cells and ON cells do not have a strong gradient, whereas there is an area of slow ON cells in the dorsal retina in terms of 1st peak time (Fig. 3.6f-h, right panels; Fig. 3.6f, middle panel). Overall, in accordance with distributions of kinetic parameters, OFF cells are significantly slower than ON everywhere in the retina.

Next, I assessed the differences between chirp responses of ON and OFF cells and the spatial organization of the responses. Firstly, I confirmed the hypothesis that the strength of a chirp response (hence, its QI) depends on the relative surround strength of the RGC in question, such that cells with uneven center and surround (relative surround strength not equals one) have on average higher chirp response QI (Fig. 3.6c). This is relevant to the question of difference in chirp response statistics between ON and OFF cells because ON cells have more cells with high QI and also their mean of relative surround strength distribution is less than one (Fig. 3.6d-e). Consequently, when mapped separately, QIs of ON and OFF cells differ drastically. OFF cells have on average very low QI (<0.3) across the entire retina (Fig. 3.6i, right panel). ON cells have a striking gradient of QIs - below the horizon line QI is low and right above the horizon it raises significantly, while ventral retina has slightly lesser QIs (Fig. 3.6i, middle panel). The change in ON cells chirp responses influences the average QI distribution in the retina accordingly (Fig. 3.6i, left panel).

In summary, in addition to previous findings on organization of spatial RFs across the retina, my analysis showed that there exist gradients of temporal response properties as well as of chirp responses, which are both likely to be linked to the uneven distribution of ON and OFF cells in the retina.

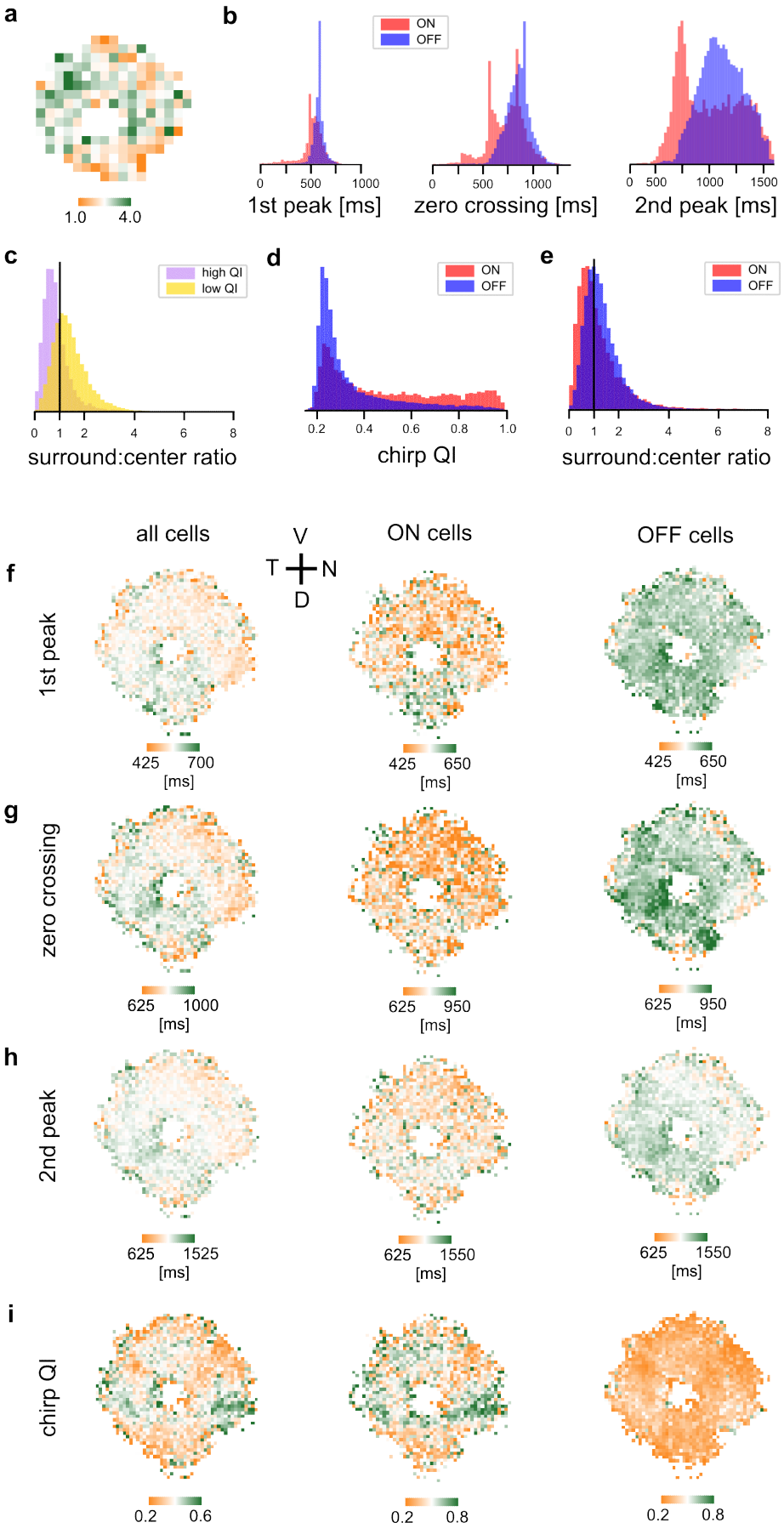
a
1.0 4.0
b
ON
OFF
0 500 1000
1st peak [ms]
0 500 1000
zero crossing [ms]
0 500 1000 1500
2nd peak [ms]
c
high QI
low QI
0 1 2 4 6 8
surround:center ratio
d
ON
OFF
0.2 0.4 0.6 0.8 1.0
chirp QI
e
ON
OFF
0 1 2 4 6 8
surround:center ratio
all cells
ON cells
OFF cells
V
T
N
D
f
1st peak
425 700 [ms]
425 650 [ms]
425 650 [ms]
g
zero crossing
625 1000 [ms]
625 950 [ms]
625 950 [ms]
h
2nd peak
625 1525 [ms]
625 1550 [ms]
625 1550 [ms]
i
chirp QI
0.2 0.6
0.2 0.8
0.2 0.8

Figure 3.6 *(preceding page)*: **Comparison of kinetics of ON and OFF cells and changes in kinetics across the retina. a.** OFF:ON cell count ratio. **b.** Distribution of timings of first peak (left panel), zero crossing (middle panel), second peak (right panel) in the temporal RFs of RGCs. **c.** Distributions of relative surround:center strength differ for cells exhibiting high-quality chirp responses and low-quality. **d.** Distributions of QIs of chirp responses differ for ON and OFF cells. **e.** Distributions of relative surround:center strength differ for ON and OFF cells. **f.** Right: map of timing of the first peak in the temporal filter for all RGCs in the dataset. Middle: same for ON cells. Left: same for OFF cells. **g.** Same as f for timing of zero crossing. **h.** Same as f for timing of the second peak. **i.** Same as f for chirp response QI. D, dorsal; V, ventral; T, temporal; N, nasal

CHAPTER 4

Discussion

In this work, we utilized a novel epi-fluorescent imaging setup (Fig. 2.1) to perform functional classification of RGCs sampled from a big FOV (Fig. 3.2, 3.3, 3.4, 3.5), and studied the global RF architecture (Fig. 3.6). Our results show the existence of pronounced variability in spatio-temporal properties of RGCs and that these properties do not seem to split into clear differentiable subgroups. Conversely, they seem to form a gradient of features (Fig. 3.5), which also leads some of the features to form a gradient across the visual field (Fig. 3.6).

4.1 Functional classification

While clustering RGCs solely based on their spatial RFs, we noticed that corresponding within cluster chirp responses vary greatly (Fig. 3.2). Consequently, clusters of chirps had cells with spatio-temporal filters of both polarities (Fig. 3.3). Additionally, I attempted reconstruction of chirp responses by convolving the temporal RFs with the chirp stimulus, and the results were disappointing for a significant fraction of the cells (data not shown). Together, these findings strengthen the argument that RGCs perform nonlinear spatial integration across their spatial RFs, and suggest that, even though with our setup we acquired RFs of unprecedented spatial resolution, spatio-temporal receptive fields describe the function of RGCs only partially [36; 37].

Clustering of spatial RFs also revealed groups of RGCs that have a pronounced bias in their distribution (Fig. 3.2c, left column). Clusters 1, 4, 12, 17 are concentrated in the dorsal part of the retina below the horizon. These clusters show a striking surround asymmetry, such that the top is stronger. In contrast, cluster 10 shows the opposite surround asymmetry and the opposite distribution pattern. Clusters 11 and 15 are interesting as well, because they have a relatively small size of center RF and are distributed in the ventral part of the retina. This is in accordance with the previous findings, which linked vertical surround asymmetry and center size with elevation of the cell within the visual field [27]. Such organization of RF architectures within the retina have been implicated with efficient coding strategies of natural scene statistics.

Another observation that caught my attention among the outcomes of functional classification is that the strongest activated-by-contrast (AbC) chirp responses come from ON cells clusters (e.g. clusters 16-20 in Fig. 3.2 and clusters 1-6 in Fig. 3.3), while the majority of cells producing suppressed-by-contrast chirp responses are OFF cells (e.g. clusters 16, 17, 19, 20 in

Fig. 3.3). Regarding AbC chirp responses, the answer seems to lie in spatial RFs of those cells. Clusters 16, 17 and 20 in Fig. 3.3, which have the most strong chirp responses, have very weak surround. A correlation between surround:center strength ratio and quality (strength) of chirp responses is shown in Fig. 3.6 and previous research [27]. This effect seems rather intuitive because the center and the surround always have opposite signs and if they are both equally strong they would cancel each other out when stimulated by a full-field signal. A similar effect can be seen in the work of Goetz et al. where some cells stopped responding to flashing spots after their size increased and supposedly became bigger than the RF center [2]. These groups of cells did not respond to spots bigger than 500 microns in diameter and most cells have their RF centers under 400 microns in diameter [1], meaning that spots of bigger diameter activate both the center and the surround.

The observed effect for SbC cells does not seem to be so easily explainable. Previous research on suppressed-by-contrast cells indicates that both ON and OFF cells are equally involved in producing such responses [38]. At the same time Jacoby et al. identified a different type of SbC response produced by ON cells [39]. To avoid the confusion, it is important to keep in mind the definition of ON and OFF cells - functionally, ON and OFF cells are responding to increase and decrease in light stimulus respectively; anatomically, their dendrites stratify in ON and OFF sublamina of inner plexiform layer. However, in this and other works ON and OFF cells are called so depending on the polarity of their temporal RF (corresponding to the polarity of the center of spatial RF). As described in the introduction chapter, temporal RF is an approximation of a light stimulus that is most likely to elicit a spike in a given cell. I argue that when it comes to SbC RGCs, it is unclear whether temporal RF is a good description of a cell's response properties since its response is absence of spiking rather than an increase in activity. Therefore, the observed effect of SbC cells being mostly OFF in terms of RF polarity can be misleading and irrelevant. Perhaps, different subtypes of RGCs benefit from different ways to describe their properties, but in this work we are mostly focusing on the receptive fields.

Overall, our data shows that there is no way to clearly divide RGCs into functional subtypes based on their spatial RFs, temporal filters and chirp responses (Fig. 3). This result was not expected, as multiple studies have shown that RGCs have a definite number of morphology types as well as genetic types, which mostly correspond with each other and with functional characteristics [2; 1; 40].

One of the reasons could be that k-means clustering is not suited for such complex data. However, hierarchical clustering, DBSCAN and HDBSCAN performed even worse and did not pick up differentiable clusters at all (data not shown). In line with these negative clustering results, when sorting all temporal filters, we can clearly observe that temporal RFs in our dataset exhibit all possible linear combinations of properties within the four main clusters of mono- and biphasic ON and OFF cells (Fig. 3.4a).

Our stimulation and recording approach, although not perfect (highly photopic conditions, only S opsin is active, full-field stimulus, no direct readout of spiking activity), is unlikely the reason for not finding clusters. Our study should be able to reproduce results of the study of Baden et al. The main difference with all the previous functional classification studies is our large FOV. Hence, our working hypothesis is that different parts of the retina contain different sets of RGC subtypes and some (or all) of these subtypes gradually change their properties across the retina. It might not be true for rod pathways, however at photopic conditions during the daylight vision natural scene statistics varies a lot across the visual field and our data suggests that the retina is utilizing functional gradients to adapt to this statistics. For

discussion of how the retina could establish such an organization of RFs see [27].

Additionally, there exists evidence that RGCs change their function with shifts in overall luminance levels [41]. I argue that this data, as well as responses to spots of changing sizes centered at the RF of each cell, should be taken into consideration when performing functional classification of RGCs. This would, of course, add even more complexity to the clusterization problem, however, perhaps the solution would be to change the focus from definitive functional clustering to groups that gradually change their properties according to the statistical needs imposed by nature.

It is also important to consider that the process of clustering entails forcing data into groups and then comparing the mean values of these groups. One can imagine a gradient of colors that is being split into groups. The mean colors representing each of these groups would obviously be different from each other, however there would still be a smooth gradient behind these enforced clusters. Our data shows that a similar thing might have been happening in the past studies on functional classification of cells, while it could be that clusters are not meaningful when it comes to the function of RGCs.

In order to prove the presence of clusters, one would have to show not only the difference between the centroids of these clusters, but also that the densities of data points around the centroids are higher than, for example, exactly between the two nearest centroids. Unless this has been proved, claims about the existence of distinct clusters must be taken with a grain of salt.

4.2 Retinal organizational patterns

Visual scenes in the sky and on the ground differ in contrast statistics: the daylight sky has high brightness and all objects appear as negative contrasts, whereas on the ground both positive and negative contrasts appear with roughly the same probability [6]. At the same time, objects in the sky have high behavioral relevance (e.g. predatory birds) and therefore should be robustly detected by the brain. Therefore, one could hypothesize that OFF cells are abundant in the region of the retina looking at the sky (ventral retina) and have a similar ratio of ON and OFF cells in the dorsal retina. This is exactly what our data shows in the OFF:ON ratio map of the retina (Fig. 3.6a).

Apart from being unevenly distributed, ON and OFF cells have different kinetics as shown in Fig. 3.6b, as well as chirp responses and spatial RFs (Fig. 3.6d,e). This could be explained by their different intrinsic electrophysiology [42; 43], however it is outside the scope of this work to prove it. What is relevant for functional characterization of RGCs is that both ON and OFF cells exhibit their temporal filtering properties non-uniformly across the retina (Fig. 3.6f-h, middle and right panels). The varying OFF:ON ratio combined with these cell types' non-uniform kinetics impose a gradient of temporal properties on the whole retina (Fig. 3.6f-h,left panels).

Moreover, I linked the strength of a cell's chirp response to the feature of its spatial RF (surround:center relative strength) and then showed that the strength of a chirp response is another parameter that forms a gradient across the retina, which is strongly pronounced around the horizon line (Fig. 3.6i).

The described gradients of RGCs kinetics and chirp responses quality, together with previously described gradient in center-surround asymmetry of spatial RFs [27], as well as my lack of

success in finding clusters among the response properties provide a strong evidence that RGCs in the retina are functionally organized in terms of gradients of features rather than functional subtypes, which could be a result of adaptation of the retina to natural scene statistics in the daylight.

To strengthen the argument that gradients of functional properties exist, one would need to devise a robust statistical test for whether a certain functional property of the RGCs is really spatially distributed as opposed to being randomly distributed.

Bibliography

[1] T. Baden, P. Berens, K. Franke, M. Román Rosón, M. Bethge, and T. Euler, "The functional diversity of retinal ganglion cells in the mouse," *Nature*, vol. 529(7586), pp. 345–350, 2016.

[2] J. Goetz, Z. F. Jessen, A. Jacobi, A. Mani, S. Cooler, D. Greer, S. Kadri, J. Segal, K. Shekhar, J. R. Sanes, *et al.*, "Unified classification of mouse retinal ganglion cells using function, morphology, and gene expression," *Cell reports*, vol. 40, no. 2, p. 111040, 2022.

[3] J. R. Sanes and S. L. Zipursky, "Design principles of insect and vertebrate visual systems," *Neuron*, vol. 66, no. 1, pp. 15–36, 2010.

[4] J. B. Demb and J. H. Singer, "Functional circuitry of the retina," *Annual review of vision science*, vol. 1, p. 263, 2015.

[5] L. D. Carter-Dawson and M. M. Lavail, "Rods and cones in the mouse retina. i. structural analysis using light and electron microscopy," *Journal of Comparative Neurology*, vol. 188, no. 2, pp. 245–262, 1979.

[6] T. Baden, T. Schubert, L. Chang, T. Wei, M. Zaichuk, B. Wissinger, and T. Euler, "A tale of two retinal domains: near-optimal sampling of achromatic contrasts in natural scenes through asymmetric photoreceptor distribution," *Neuron*, vol. 80, no. 5, pp. 1206–1217, 2013.

[7] T. Euler, S. Haverkamp, T. Schubert, and T. Baden, "Retinal bipolar cells: elementary building blocks of vision," *Nature Reviews Neuroscience*, vol. 15, no. 8, pp. 507–519, 2014.

[8] S. A. Bloomfield and R. F. Dacheux, "Rod vision: pathways and processing in the mammalian retina," *Progress in retinal and eye research*, vol. 20, no. 3, pp. 351–384, 2001.

[9] T. Baden, P. Berens, M. Bethge, and T. Euler, "Spikes in mammalian bipolar cells support temporal layering of the inner retina," *Current Biology*, vol. 23, no. 1, pp. 48–52, 2013.

[10] C. A. Chapot, T. Euler, and T. Schubert, "How do horizontal cells 'talk'to cone photoreceptors? different levels of complexity at the cone–horizontal cell synapse," *The Journal of physiology*, vol. 595, no. 16, pp. 5495–5506, 2017.

[11] W. Yan, M. A. Laboulaye, N. M. Tran, I. E. Whitney, I. Benhar, and J. R. Sanes, "Mouse retinal cell atlas: molecular identification of over sixty amacrine cell types," *Journal of Neuroscience*, vol. 40, no. 27, pp. 5177–5195, 2020.

[12] J. S. Diamond, "Inhibitory interneurons in the retina: types, circuitry, and function," *Annu Rev Vis Sci*, vol. 3, no. 1, pp. 1–24, 2017.

[13] L. P. Morin and K. M. Studholme, "Retinofugal projections in the mouse," *Journal of Comparative Neurology*, vol. 522, no. 16, pp. 3733–3753, 2014.

[14] J. A. Bae, S. Mu, J. S. Kim, N. L. Turner, I. Tartavull, N. Kemnitz, C. S. Jordan, A. D. Norton, W. M. Silversmith, R. Prentki, *et al.*, "Digital museum of retinal ganglion cells with dense anatomy and physiology," *Cell*, vol. 173, no. 5, pp. 1293–1306, 2018.

[15] U. S. Kim, O. A. Mahroo, J. D. Mollon, and P. Yu-Wai-Man, "Retinal ganglion cells—diversity of cell types and clinical relevance," *Frontiers in Neurology*, p. 635, 2021.

[16] E. Soucy, Y. Wang, S. Nirenberg, J. Nathans, and M. Meister, "A novel signaling pathway from rod photoreceptors to ganglion cells in mammalian retina," *Neuron*, vol. 21, no. 3, pp. 481–493, 1998.

[17] S. E. Hausselt, T. Euler, P. B. Detwiler, and W. Denk, "A dendrite-autonomous mechanism for direction selectivity in retinal starburst amacrine cells," *PLoS biology*, vol. 5, no. 7, p. e185, 2007.

[18] A. Krishnaswamy, M. Yamagata, X. Duan, Y. K. Hong, and J. R. Sanes, "Sidekick 2 directs formation of a retinal circuit that detects differential motion," *Nature*, vol. 524, no. 7566, pp. 466–470, 2015.

[19] M. V. Srinivasan, S. B. Laughlin, and A. Dubs, "Predictive coding: a fresh view of inhibition in the retina," *Proceedings of the Royal Society of London. Series B. Biological Sciences*, vol. 216, no. 1205, pp. 427–459, 1982.

[20] S. Wienbar and G. W. Schwartz, "The dynamic receptive fields of retinal ganglion cells," *Progress in retinal and eye research*, vol. 67, pp. 102–117, 2018.

[21] J. Y. Lettvin, H. R. Maturana, W. S. McCulloch, and W. H. Pitts, *What the frog's eye tells the frog's brain*. na, 1965.

[22] H. B. Barlow *et al.*, "Possible principles underlying the transformation of sensory messages," *Sensory communication*, vol. 1, no. 01, 1961.

[23] S. Laughlin, "A simple coding procedure enhances a neuron's information capacity," *Zeitschrift für Naturforschung c*, vol. 36, no. 9-10, pp. 910–912, 1981.

[24] V. Balasubramanian and P. Sterling, "Receptive fields and functional architecture in the retina," *The Journal of physiology*, vol. 587, no. 12, pp. 2753–2767, 2009.

[25] K. M. Ahmad, K. Klug, S. Herr, P. Sterling, and S. Schein, "Cell density ratios in a foveal patch in macaque retina," *Visual neuroscience*, vol. 20, no. 2, pp. 189–209, 2003.

[26] G. Tkačik, J. S. Prentice, J. D. Victor, and V. Balasubramanian, "Local statistics in natural scenes predict the saliency of synthetic textures," *Proceedings of the National Academy of Sciences*, vol. 107, no. 42, pp. 18149–18154, 2010.

[27] D. Gupta, W. Mlynarski, O. Symonova, J. Svaton, and M. Joesch, "Panoramic visual statistics shape retina-wide organization of receptive fields," *bioRxiv*, 2022.

[28] P. Bethge, S. Carta, D. A. Lorenzo, L. Egolf, D. Goniotaki, L. Madisen, F. F. Voigt, J. L. Chen, B. Schneider, M. Ohkura, *et al.*, "An r-camp1. 07 reporter mouse for cell-type-specific expression of a sensitive red fluorescent calcium indicator," *PloS one*, vol. 12, no. 6, p. e0179460, 2017.

[29] M. Pachitariu, C. Stringer, M. Dipoppa, S. Schröder, L. F. Rossi, H. Dalgleish, M. Carandini, and K. D. Harris, "Suite2p: beyond 10,000 neurons with standard two-photon microscopy," *BioRxiv*, p. 061507, 2017.

[30] D. H. Brainard and S. Vision, "The psychophysics toolbox," *Spatial vision*, vol. 10, no. 4, pp. 433–436, 1997.

[31] L. McInnes, J. Healy, and J. Melville, "Umap: Uniform manifold approximation and projection for dimension reduction," *arXiv preprint arXiv:1802.03426*, 2018.

[32] B. Richardson, B. Rees, T. Drabas, E. Oldridge, D. A. Bader, and R. Allen, "Accelerating and expanding end-to-end data science workflows with dl/ml interoperability using rapids," in *Proceedings of the 26th ACM SIGKDD International Conference on Knowledge Discovery & Data Mining*, pp. 3503–3504, 2020.

[33] F. Pedregosa, G. Varoquaux, A. Gramfort, V. Michel, B. Thirion, O. Grisel, M. Blondel, P. Prettenhofer, R. Weiss, V. Dubourg, *et al.*, "Scikit-learn: Machine learning in python," *the Journal of machine Learning research*, vol. 12, pp. 2825–2830, 2011.

[34] T. M. Kodinariya and P. R. Makwana, "Review on determining number of cluster in k-means clustering," *International Journal*, vol. 1, no. 6, pp. 90–95, 2013.

[35] Y. Wang and H. Zhao, "Non-linear archetypal analysis of single-cell rna-seq data by deep autoencoders," *PLoS computational biology*, vol. 18, no. 4, p. e1010025, 2022.

[36] D. Karamanlis and T. Gollisch, "Nonlinear spatial integration underlies the diversity of retinal ganglion cell responses to natural images," *Journal of Neuroscience*, vol. 41, no. 15, pp. 3479–3498, 2021.

[37] J. K. Liu, D. Karamanlis, and T. Gollisch, "Simple model for encoding natural images by retinal ganglion cells with nonlinear spatial integration," *PLoS computational biology*, vol. 18, no. 3, p. e1009925, 2022.

[38] N.-W. Tien, J. T. Pearson, C. R. Heller, J. Demas, and D. Kerschensteiner, "Genetically identified suppressed-by-contrast retinal ganglion cells reliably signal self-generated visual stimuli," *Journal of Neuroscience*, vol. 35, no. 30, pp. 10815–10820, 2015.

[39] J. Jacoby, Y. Zhu, S. H. DeVries, and G. W. Schwartz, "An amacrine cell circuit for signaling steady illumination in the retina," *Cell reports*, vol. 13, no. 12, pp. 2663–2670, 2015.

[40] W. Huang, Q. Xu, J. Su, L. Tang, Z.-Z. Hao, C. Xu, R. Liu, Y. Shen, X. Sang, N. Xu, *et al.*, "Linking transcriptomes with morphological and functional phenotypes in mammalian retinal ganglion cells," *Cell Reports*, vol. 40, no. 11, p. 111322, 2022.

[41] A. Tikidji-Hamburyan, K. Reinhard, H. Seitter, A. Hovhannisyan, C. A. Procyk, A. E. Allen, M. Schenk, R. J. Lucas, and T. A. Münch, "Retinal output changes qualitatively with every change in ambient illuminance," *Nature neuroscience*, vol. 18, no. 1, pp. 66–74, 2015.

[42] T. Kameneva, H. Meffin, and A. N. Burkitt, "Modelling intrinsic electrophysiological properties of on and off retinal ganglion cells," *Journal of computational neuroscience*, vol. 31, no. 3, pp. 547–561, 2011.

[43] D. J. Margolis and P. B. Detwiler, "Different mechanisms generate maintained activity in on and off retinal ganglion cells," *Journal of Neuroscience*, vol. 27, no. 22, pp. 5994–6005, 2007.